Predicting Extreme Phases of the Indian Summer Monsoon*

QINGHUA DING AND BIN WANG+

Department of Meteorology, School of Ocean and Earth Science and Technology, University of Hawaii at Manoa, Honolulu, Hawaii

(Manuscript received 29 January 2008, in final form 17 July 2008)

ABSTRACT

Extreme active and break phases of the Indian summer monsoon (ISM) often bring about devastating floods and severe draughts. Here it is shown that these extreme phases exhibit distinctive precursory circulation conditions in both the tropics and extratropics over a range of antecedent periods. The extremely active monsoon over northern India is preceded by a strengthening of the upper-tropospheric central Asian high and enhancement of the tropical convection over the equatorial Indian Ocean and the South China Sea. The concurrent buildup of the anomalous high over central Asia and the arrival of tropical convection over northern India increase the likelihood of occurrence of a heavy rainy period there. Similarly, the concurrent anomalous low over central Asia and the arrival of suppressed convection originating from the equatorial Indian Ocean and the South China Sea precede extremely strong monsoon breaks over northern India. Two predictors can be used to predict the extreme active/break phases of the northern ISM: normalized 200-hPa geopotential height over central Asia and outgoing longwave radiation over southern India. Once the mean of the two predictors exceeds a threshold unit (1.0), an extreme phase is anticipated to occur over northern India after 4–5 days and reach peak intensity after an additional 2 days. In general, an event forecast by this simple scenario has a 40% probability of developing into an extreme phase, which is normally a small probability event (a less than 4% occurrence).

1. Introduction

More than a billion people live in India, which is a typical monsoon region with a high, increasing population density. Situated at the heart of the Indian summer monsoon (ISM) region, the Indian subcontinent experiences vigorous intraseasonal variability during the summer, with quasi-periodic wet episodes (''active'' phases) and dry episodes (''break'' phases; Raghavan 1973; Krishnan et al. 2000; Gadgil and Joseph 2003; Krishnamurthy and Shukla 2007, 2008; Rajeevan et al. 2008). The public safety and economy of India are very vulnerable to the occurrence of extreme active and break phases of the ISM intraseasonal oscillation (ISO; Gadgil 1995; Sikka 1999; Webster et al. 1998; Gadgil and Rao 2000; Gadgil et al. 2002; Webster and Hoyos 2004; De et al. 2005), which give rise to devastating floods, landslides, and prolonged, severe droughts. As the latest example of an extremely active phase, torrential monsoon rains caused widespread floods throughout India and Pakistan from late July through mid-August 2006. In India, hundreds of people and tens of thousands of animals died, and more than 6 million people were affected by the floods. In Pakistan, monsoon-related flooding was blamed for more than 230 deaths (Bell et al. 2006).

Obviously, understanding the cause of the extreme active/break monsoon phases is of great importance, and accurate prediction thereof can minimize the damage to life and property. Unfortunately, little has been known about the causes of the extreme active and break phases of the ISM. This study is aimed at filling in this knowledge gap.

The boreal summer ISO over India has long been regarded as a source of active and break phases of the

* School of Ocean and Earth Science and Technology Publication Number 7507 and International Pacific Research Center Publication Number 536.

+ Additional affiliation: International Pacific Research Center, School of Ocean and Earth Science and Technology, University of Hawaii at Manoa, Honolulu, Hawaii.

Corresponding author address: Dr. Qinghua Ding, Department of Meteorology, School of Ocean and Earth Science and Technology, University of Hawaii at Manoa, 2525 Correa Road, Honolulu, HI 96822.
E-mail: qinghua@hawaii.edu

DOI: 10.1175/2008JCLI2449.1

ISM. The ISO over South Asia shows significant double spectral peaks at 30–60 and 10–20 days (Krishnamurti and Bhalme 1976; Sikka and Gadgil 1980; Murakami et al. 1984; Hartmann and Michelson 1989; Annamalai and Slingo 2001). The former propagates northward from the equatorial Indian Ocean to northern India, while the latter often propagates westward from the South China Sea to the Indian subcontinent; both have been recognized as the dominant modulator for the active and break cycles of the ISM (Goswami 2005).

However, the tropical ISOs are not the only drivers; atmospheric circulation anomalies originating from midlatitudes can also affect the intraseasonal variability of the ISM. The pioneering work by Ramaswamy (1962) establishes the linkage of an ISM break with the southward-penetrating midtropospheric westerly trough into the Indo-Pakistan region. He noted that a penetration of a midlatitude Rossby wave train can weaken the Tibetan high and the upper-level easterlies. The weakening and bifurcation of the Tibetan high during the weak ISM period under the influence of a midlatitude trough was also reported by Unninayar and Murakami (1978). Case studies by Raman and Rao (1981) noted the existence of two upper-tropospheric blocking ridges situated over the North Caspian Sea and eastern Siberia during severe drought years of the ISM. For active phases of the ISM, Kripalani et al. (1997) considered the upper-tropospheric ridge to the northwest of India as a sign of the active monsoon over northern and central India. Recent observation by Ding and Wang (2007) reveals an intraseasonal trans-Eurasia teleconnection pattern; an anomalous high pressure in the upper troposphere appears to occur initially in northwestern Europe, forming a Rossby wave train that propagates southeastward toward central Asia, and then travels along the westerly jet stream farther toward East Asia and the western North Pacific. Once the anomalous high pressure occurs over central Asia, it can excite significant convection anomalies over northern India and Pakistan.

Thus, the intraseasonal variability of the ISM is influenced by the disturbances coming from both the tropics and the extratropics. It is conceivable that the collaborative impact of the tropical ISO and extratropical wave train may increase the likelihood of extreme active and break ISM phases. In this study we explore the relationships between tropical intraseasonal variability, the midlatitude circulation, and the extreme active and break phases of the ISM during boreal summer (June–September). We found prominent precursors for the extreme active and break phases of the ISM in the both the tropics and extratropics. An attempt is made to relate the probability of the occurrence of extreme ISO phases to the tropical–extratropical interaction. The implication of the result on the prediction and predictability of the ISM ISO is discussed.

2. Data and strategy

a. Data

The major dataset used in this work was of the daily averages of outgoing longwave radiation (OLR) on a 2.5° square grid, obtained through the National Oceanic and Atmospheric Administration satellite, and daily mean National Centers for Environmental Prediction (NCEP)/Department of Energy Global Reanalysis 2 (NCEP-2) data on a $2.5° \times 2.5°$ grid at standard pressure levels (Kanamitsu et al. 2002). For simplicity of the interpretation, the sign of OLR anomalies is reversed so that the positive OLR anomalies represent enhancement of convective activity. To estimate the rainfall intensity during the extreme phase, rainfall data from the Climate Prediction Center (CPC) Merged Analysis of Precipitation (CMAP; Xie and Arkin 1997) were employed. The CMAP data were interpolated from pentad means to daily values. In addition, Global Precipitation Climatology Project (GPCP) daily precipitation ($1.0° \times 1.0°$) (Huffman et al. 2001) and high resolution ($1.0° \times 1.0°$), gridded daily rainfall over India developed by the India Meteorological Department (Rajeevan et al. 2006) were compared with the OLR field to verify the ability of OLR in measuring rainfall variability over the Indian monsoon region.

b. Time filter scheme

Both OLR and NCEP-2 data cover 28 consecutive boreal summers (defined as the 122-day period from 1 June through 30 September) from 1979 to 2006. A three-step temporal filtering scheme was applied to daily data to obtain the intraseasonal variability to the largest extent. First, a 28-summer-averaged, least squares–fitting parabola was removed from the unfiltered data to eliminate the climatological seasonal cycle. Then, the mean of each season was removed in order to retain only weather and intraseasonal variability. Finally, a 5-day running mean time filter was applied to the daily data to eliminate weather variability and retain intraseasonal variability longer than 10 days. To preserve intraseasonal variability as much as possible, no other filter was applied to the data. The filtered intraseasonal data were used for correlation analysis, composite analysis, and hindcast experiment for the extreme phases.

c. Definition of the extreme phase

The active and break ISM conditions are traditionally defined based on the location of monsoon trough and

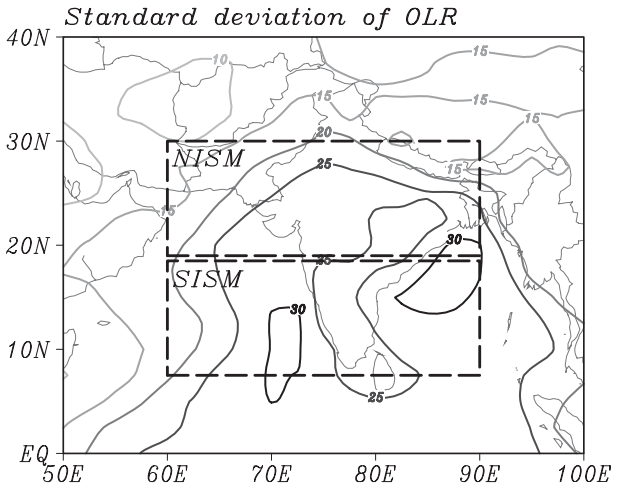

FIG. 1. Standard deviation of the daily OLR (color contours with an interval of 5 W m^{-2}) for 28 summers (1June–30 September). OLR is used as a proxy for convection and the daily OLR is filtered intraseasonal component. The domains for the NISM (20°–30°N, 60°–90°E) and SISM (7.5°–17.5°N, 60°–90°E) are denoted by dashed lines.

precipitation criterion over central India (Ramamurthy 1969; Rao 1976; Krishnan et al. 2000; Goswami 2005). To capture the large-scale circulation variability, circulation indices are also commonly used to define the active and break ISM conditions (Webster et al. 1998; Goswami and Mohan 2001). In this study, we use OLR to identify the large-scale convective signature of active and break phases.

Ding and Wang (2007) proposed a positive interaction between the midlatitude wave train and convection anomalies over the northern India and Pakistan. We may expect that this tropical–extratropical interaction has more significant impacts over the northern ISM domain and less in the southern part. With this consideration in mind, division of the ISM domain into northern and southern parts is essential to test whether the effects of the tropical–extratropical interaction on extreme phases on the northern and southern ISM are different.

A daily northern ISM (NISM) OLR index was defined by using the daily OLR averaged over the 20°–30°N, 60°–90°E region (Fig. 1). Similarly, a southern ISM (SISM) OLR index was defined by the daily OLR averaged in the 7.5°–17.5°N, 60°–90°E region. The two index domains cover the major intraseasonal variability centers in the ISM region (Fig. 1). Compared to the traditional precipitation criterion focusing on central India, the domains of NISM and SISM extend westward to 60°E. The new domains can additionally capture the intraseasonal variability over the Arabian Sea associated with the northward-propagating 30–60-day ISO mode and convection variability over Pakistan, which also suffers prominent flood and drought episodes during the summer season.

The extreme active and break phases of ISO were selected by using the time series of the NISM and SISM OLR. Normally, one standard deviation is used as the threshold value to define active and break phases of the ISM. On average, two to three active/break phases occur in each summer resulting from dominance of a 30–60-day ISO. In the past 28 yr, there were total of 70–80 active/break phases. In this study, we defined the top 30%–40% of the total active/break events as the extreme events. This definition can be simply fulfilled by using 1.7 standard deviation of NISM and SISM OLR to distinguish extreme events from the rest. The duration of the extreme phases were determined by the periods during which the amplitude exceeded 1.7 standard deviations. During the 28-yr period studied, there were 35 extremely active phases and 29 extreme break phases of the NISM, with an average of about 1.25 extremely active phases and one extreme break phase each year. The average duration of each extreme phase is about 4–5 days, with the peak day in the middle. Thus, the occurrence of the extreme phase is a small probability event and difficult to forecast on a daily basis. In addition, for these extreme phases, we define those active and break phases for which the amplitude of the indices exceeds 1.0 but falls below 1.7 standard deviations as strong active and break phases. There were 50 strong active phases and 57 strong break phases for the NISM during 1979–2006. Treating convective condition separately for extreme and strong categories is necessary in order to reveal the effect of tropical–extratropical interaction on the ISM phase.

d. Ability of OLR in capturing extreme phases of the ISM

The daily rainfall over the ISM domain is the best parameter to define the active and break phases of the ISO. However, the most current rainfall data available have either more or less limitation to reflect the large-scale feature of the active/break phase of the ISM in a climatological sense. Gridded Indian daily rainfall derived from stations' rainfall gauges only covers India. The extreme phase based on this gridded Indian daily rainfall may lose some large-scale features and overlook the ISO signal over Pakistan, where strong intraseasonal variability also dominates during summer season. GPCP daily rainfall data cover the entire ISM domain, but are only available for 10 yr after 1997, which is too short to provide enough sample size. Thus,

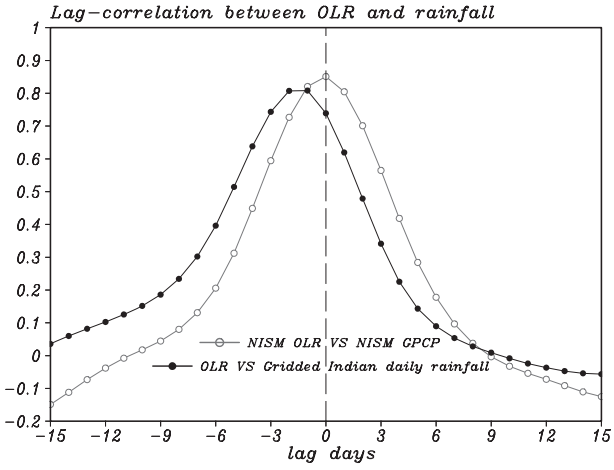

FIG. 2. Lead–lag correlation coefficients between daily OLR and GPCP data over the NISM region (gray curve with open circle) for 10 summers (1997–2006) and daily OLR and gridded Indian rainfall over northern India (black curve with filled circle) for 25 summers (1979–2003). Here, northern India is defined as the region between 20° and 30°N and west of 90°E within India. Lead–lag correlation coefficients with a lag of up to 15 days were calculated. A negative lag represents that OLR leads rainfall. The summer season is defined by the 122-day period from 1 June through 30 September. The filtered intraseasonal component of the daily OLR and rainfall were used.

OLR data are an alternative option to define extreme active/break phase of the ISM.

The lead–lag correlation coefficients between daily OLR and GPCP data for 10 summers (1997–2006) show that the highest correlation coefficient is 0.84 over the NISM at zero lag (Fig. 2). The highest correlation coefficient is 0.8 between daily OLR and gridded Indian rainfall over northern India over 25 summer (1979–2003), which occurs when OLR lead rainfall by 1 day (Fig. 2). It should be noted that the gridded Indian rainfall for a particular day measures the rainfall amount during the 24 h ending at 8030 Indian standard time. Hence, it actually records the rainfall of the previous day. It is reasonable to find a 1-day lag between satellite measurements and rainfall gauge measurements. Overall, the OLR can be used as a sensitive indicator of the large-scale convection and precipitation over the NISM region. Using 1.7 standard deviation as a threshold value, the extreme phases selected by NISM OLR and rainfall data (GPCP and Indian daily rainfall) have almost 70%–80% overlapping. Compared with the prominent active and break episodes of the ISM identified by previous study (Gadgil and Joseph 2003; Rajeevan et al. 2008; Joseph et al. 2008), it is noted that there is large overlapping (60%) between our selected cases and their well-recognized cases, although the domain is somewhat different. Based on these comparisons, we are confident that OLR with an extremely large magnitude is, to a large degree, equivalent to an extreme amount of rainfall over the NISM region.

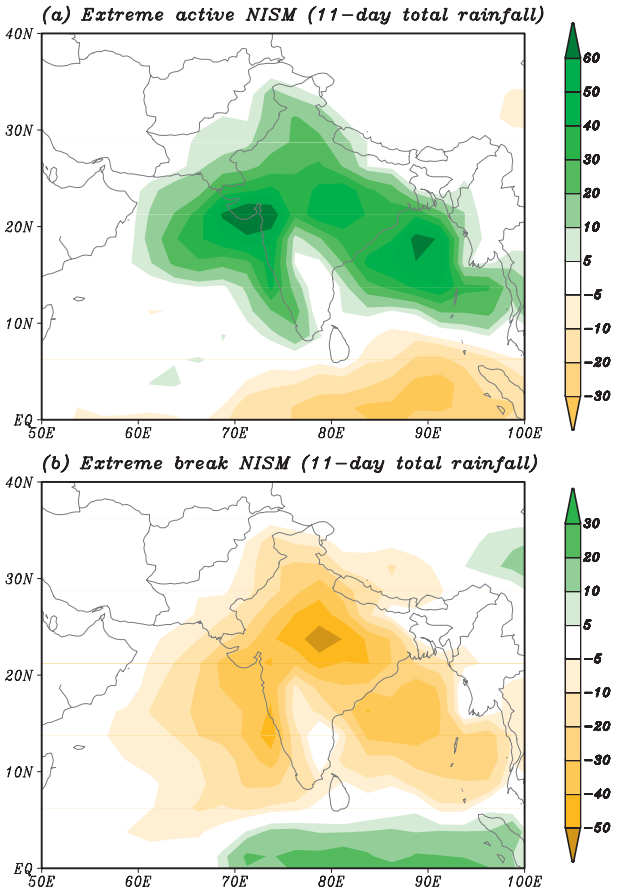

FIG. 3. The composite 11-day accumulated rainfall anomalies centered at the peak day with respect to the (a) NISM extremely active phases and (b) the NISM extreme break phases. The rainfall data are derived from CMAP.

3. Composite for extreme phases

During the NISM extreme phases, the monsoon system induces many rainfall anomalies across the whole country, especially over central and northern India (Fig. 3). Within a window of 11 days that surrounds the peak day of an extremely active phase, central India receives an excessive 40-mm accumulated rainfall, which is about a 70%–80% increase from normal rainfall; this excess often generates primary natural hazards to the local communities. On the other hand, an extreme break phase induces a 40–50-mm deficient rainfall over the central and northern regions, and the dry condition over northern India can last for a month, amplifying the aridity.

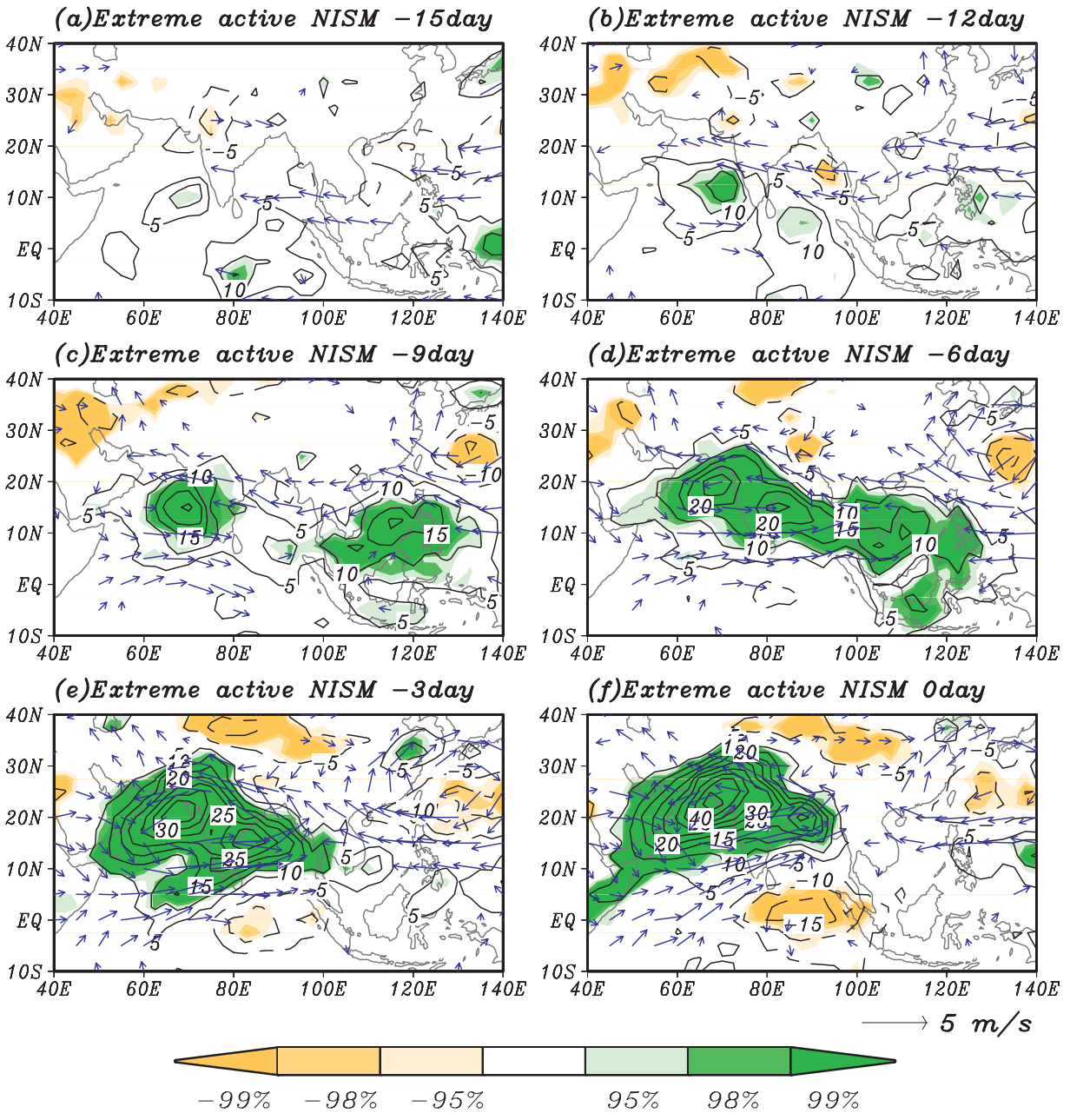

FIG. 4. The time sequence of the composite OLR (black contour s at the interval of 5 W m^{-2}) and 700-hPa wind (blue vectors) anomalies from Day −15 to Day 0 for the 35 extremely wet NISM phases. Day 0 indicates the peak wet-phase day. The shading represents OLR anomalies significant at the 95% confidence level based on Student's *t* test. Winds with both zonal and meridional components insignificant at the 95% confidence level are omitted. The sign of OLR anomalies is reversed so that the positive OLR anomalies represent enhanced convective activity.

To identify the major anomalous atmospheric conditions that precede these extreme phases, we have examined composites of tropical OLR and upper-level midlatitude circulation prior to the occurrence of the peak day (day 0). The statistical significance of the composite anomalies was assessed using Student's *t* test (Wilks 1995). The composite OLR and 700-hPa wind anomalies for 35 extremely active phases starting from 15 days prior (day −15) to day 0 were constructed (Fig. 4). The initiation of extremely wet phases is marked by the appearance of significant convection anomalies in the eastern equatorial Indian Ocean (EIO) and offshore of

the west coast of the Indian peninsula at 10°N (from day −15 to day −12). In the ensuing 6 days, the strong convection over the Indian Ocean migrates northward to the Indian subcontinent and merges with the convection band originating from the South China Sea (SCS) to establish an elongated and slanted convection zone spanning from the Arabian Sea to the western North Pacific. From day −3 to day 0, the northward-propagating tropical ISO approaches its northernmost location, and convective anomalies in the NISM region reach their maximum intensity at day 0. The amplitude of composite OLR variation at day 0 is about 30–40 W m^{-2} in the NISM, which is equivalent to about 5–7 mm day^{-1} in CMAP rainfall anomalies. The associated 700-hPa flow is characterized by a strong cyclonic circulation moving northward from the EIO to India and the Arabian Sea. The composite picture bears close resemblance to the observed canonical northward-propagating 30–60-day ISO events, which were extensively studied in previous works (e.g., Yasunari 1979, 1980, 1981; Sikka and Gadgil 1980; Krishnamurti and Subrahmanyam 1982; Wang and Rui 1990; Kemball-Cook and Wang 2001). Note that in addition to the northward movement of the ISO, a 10–20-day ISO event propagating westward from the SCS to the Bay of Bengal contributes to the extreme convection over the NISM (Fig. 4).

Figure 5 shows the composite evolution of the upper-level extratropical circulation across Eurasia from day −15 to day 0. The existence of an upper-tropospheric wave train emanating from northwestern Europe to central Asia is clearly seen 12 days prior to the peak day of an extremely wet phase. From day −9 to day −6, subsequent propagation of the wave train along the westerly jet stream to East Asia and farther extension to the North Pacific is observed. Accompanying the northward propagation of the tropical convection band into the NISM region from day −6 to day −3, the southward and eastward propagation of an upper-level wave train from the western Siberian plain to central Asia enhances the anticyclonic circulation anomalies to the north of the NISM region. The height anomalies over central Asia reach peak intensity on day −3, leading peak convection in the NISM by 3 days.

The evolution of this wave train and the role of the enhanced central Asian high in leading the strong convection over the NISM region are very similar to the behavior of midlatitude–ISM interaction described in Ding and Wang (2007). In their study, a mechanism is proposed to explain the antecedent role of the enhanced central Asian high to the convection over the NISM. To the south of the anomalous central Asian high, the easterly anomalies in the upper troposphere strengthen the easterly vertical shear over the NISM region; this increased easterly vertical shear traps the Rossby wave in the lower troposphere, which enhances convective interaction with dynamics through boundary layer convergence and increases the moist baroclinic instability, thereby increasing monsoon precipitation. This easterly vertical shear mechanism was originally proposed by Wang and Xie (1996) and Xie and Wang (1996). On the other hand, the diabatic heating anomalies associated with increased precipitation over the NISM may likely induce a baroclinic Rossby wave response to the west of the heating source, which reinforces the central Asian high at the upper troposphere (Gill 1980; Rodwell and Hoskins 1996). A positive feedback between the strengthened central Asian high and increased precipitation over the NISM manifest the active role of tropical–extratropical interaction over the NISM.

Note that the extremely active NISM is immediately preceded by the following two major atmospheric processes: 1) the merger of the northward-propagating convection anomalies originating from the eastern EIO and the westward-propagating convection anomalies from the SCS, and 2) the establishment of the strong central Asian high pressure anomalies associated with the Rossby wave train propagation from northwestern Europe. The NISM's extremely active phases tend to occur when the development of an upper-level high anomaly over central Asia coincides with the arrival of a convection zone from the EIO and the SCS. Because both the enhanced central Asian high and tropical convection anomalies can lead to an active phase of the NISM alone, the mutual aid between these two systems tends to provide a condition favorable for the occurrence of an extremely active phase.

Similarly, the composite of midlatitude circulation and OLR for 29 extreme break phases also suggests that for the occurrence of an extremely dry NISM phase, the concurrence of the following two elements is important: the anomalous upper-level central Asian cyclonic circulation combined with the suppressed convections associated with 30–60- and 10–20-day ISOs (Figs. 6 and 7). The flow patterns for extreme break phases resemble those associated with extremely active phases, except that the magnitude of the anomalous central Asian circulation for break phases is stronger. Coinciding with the northward/westward propagation of the large-scale dry zone from the EIO/SCS to the NISM (Fig. 6), a large-scale stationary Rossby wave train yielding arch-shaped propagation migrates from northwestern Europe to central Asia via the western Siberia Plain (Fig. 7). The combined effect of the anomalous low over central Asia and the dry phase of tropical ISOs are essential for

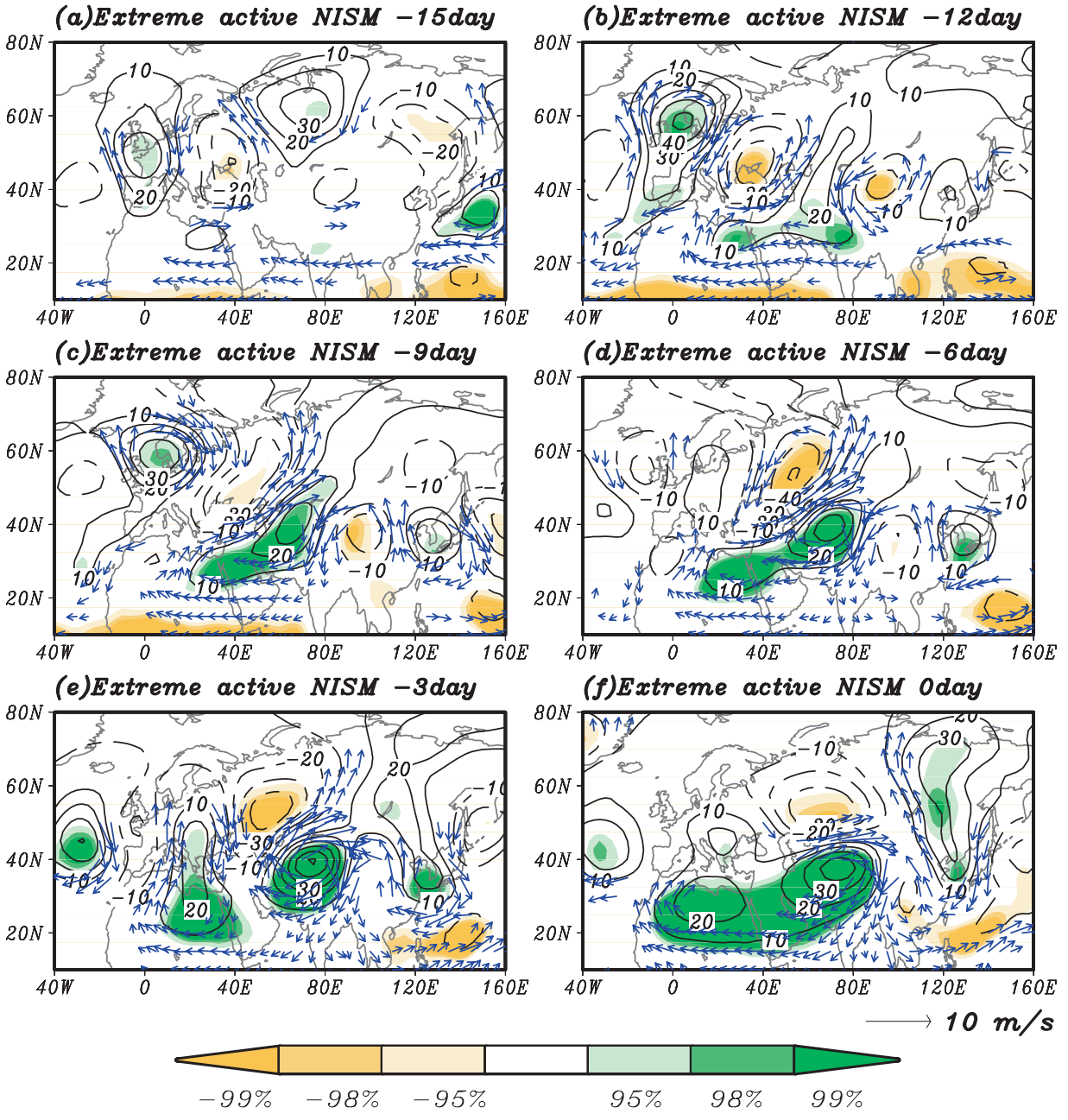

FIG. 5. As in Fig. 4, but for the 200-hPa geopotential height (black contours with interval of 10 m) and 200-hPa wind (blue vectors) anomalies.

the development of an extremely dry condition over the NISM.

The composite figures suggest that extreme phases of the SISM are subject to considerable modulation from tropical 30–60-day ISO events that are initiated over the EIO about 10 days prior to the extreme phase. There is no significant precursor for the SISM extreme phases in the extratropics. For extreme phases of the SISM, the systems from the tropics and extratropics are generally decoupled, suggesting that the anomalous circulation over central Asia is not sufficiently strong to influence the convection over the southern part of the ISM domain.

4. Importance of the timing of tropical–extratropical interaction

The results presented in the preceding section reveal that the midlatitude wave train originating from

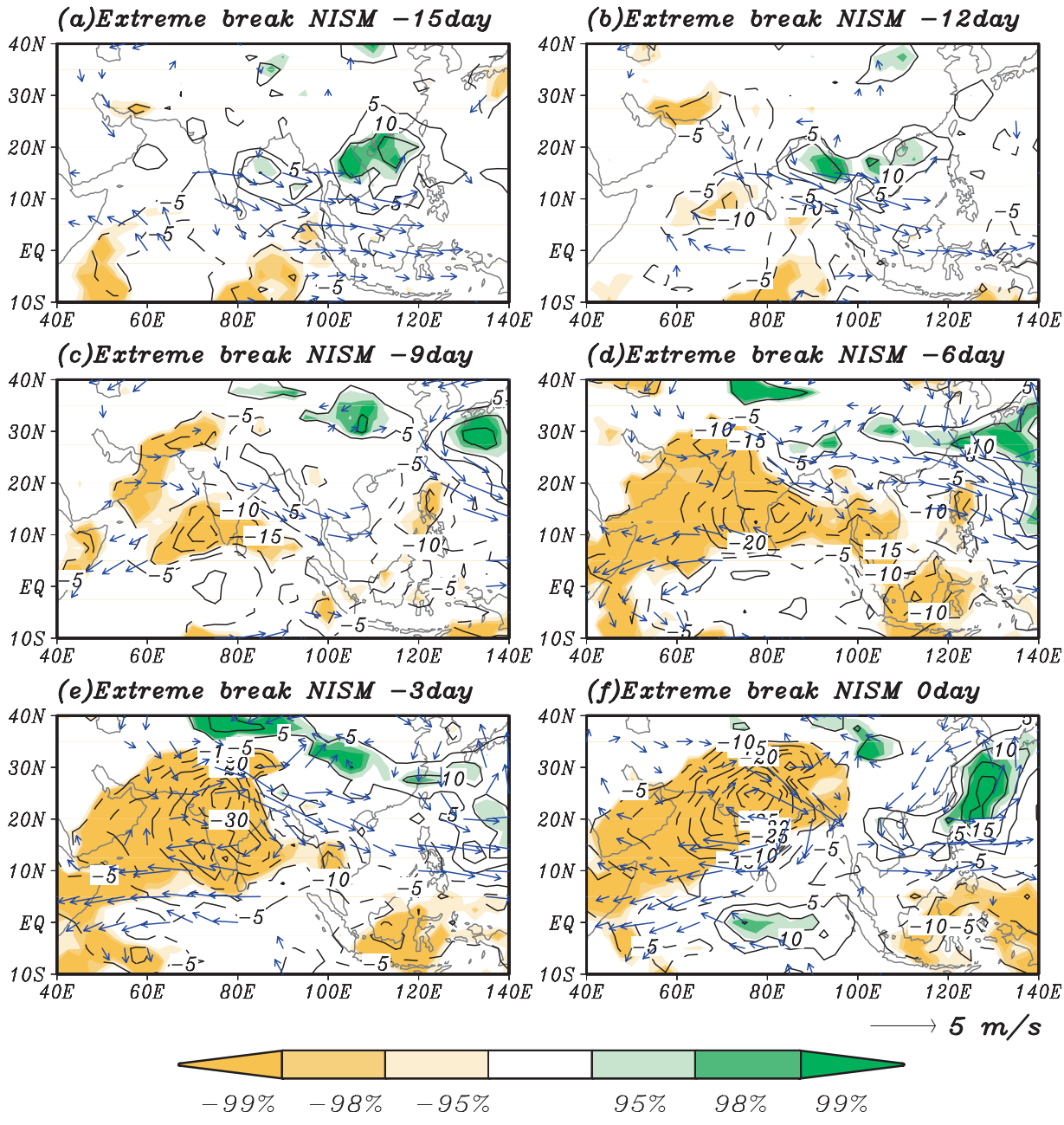

FIG. 6. As in Fig. 4, but for the 29 NISM extreme break phases.

northwestern Europe is a significant driver of ISO-related convective variability over the NISM region. However, it is not clear how the intraseasonal wave train is initiated in northwestern Europe. According to Ding and Wang (2007), the maximum intraseasonal variance of the upper-tropospheric circulation is located in northwestern Europe, and also in the exit region of the Atlantic jet stream, where strong barotropic instability of the summer mean flow dominates. The circulation anomalies over northwestern Europe, which can be considered as the origin of the midlatitude wave train, are presumably excited by efficient kinetic energy extraction from the basic state. It is speculated that the upstream tropical or extratopical forcing along the jet stream over the Atlantic Ocean, the United States, and the Pacific Ocean can excite this initial cell of the midlatitude wave train over northwestern Europe.

To gain deeper insight into how the circulation anomalies over the source region of midlatitude wave

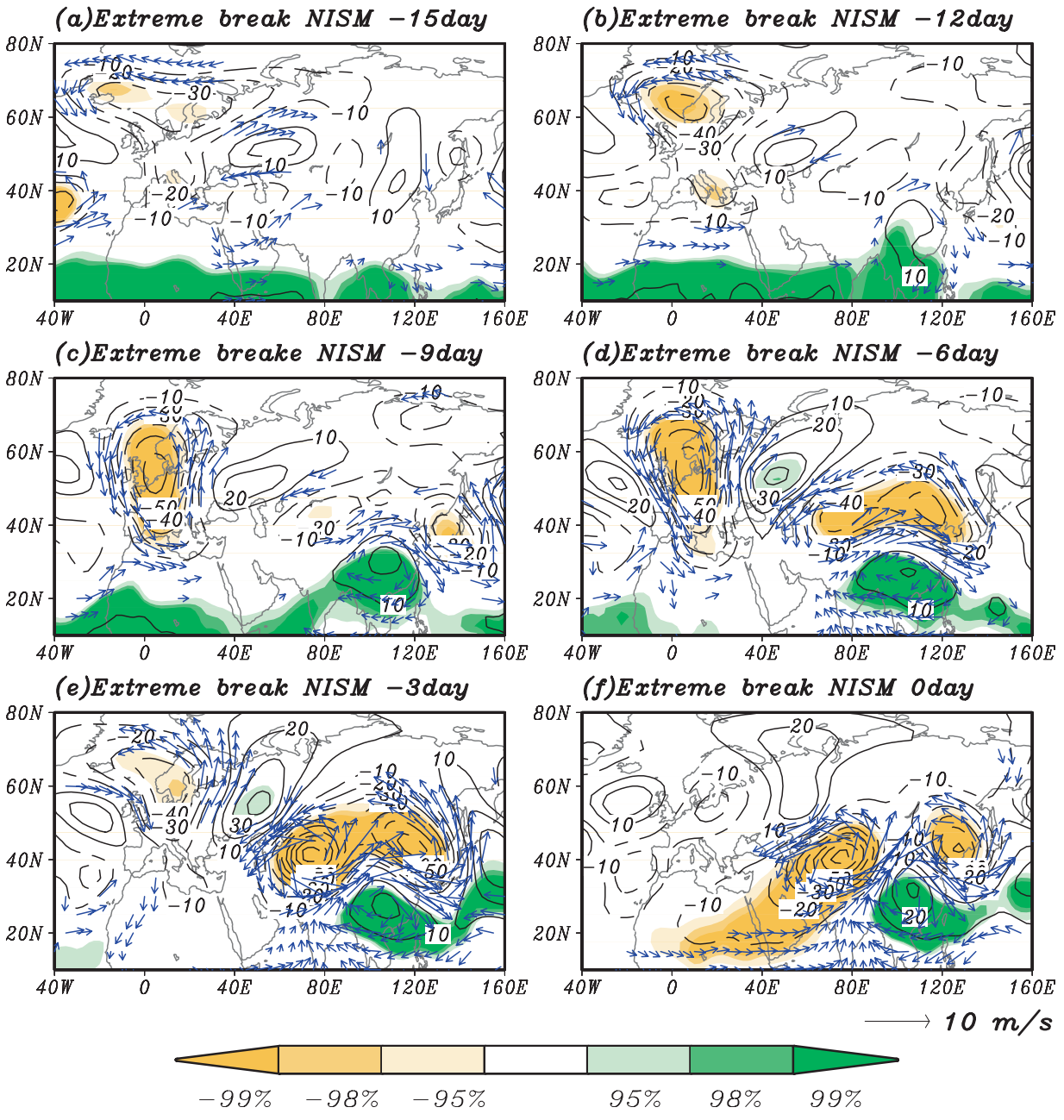

FIG. 7. As in Fig. 5, but for the 29 NISM extreme break phases.

train is related to the convection anomalies over the reinitiation region of the 30–60-day ISO events, the lead–lag correlations between northwestern Europe (50°–65°N, 5°W–15°E) 200-hPa geopotential height and OLR over the eastern EIO (5°S–5°N, 80°–90°E) were calculated with a lead and lag of up to 20 days. The variability over the two source regions did not show any significant relationship. Thus, the initiation of the midlatitude wave train is not physically linked with the initiation of the 30–60-day ISO events over the eastern EIO. The latter is likely governed by a basin-wide self-induction mechanism confined to the Indian Ocean (Wang et al. 2005; Jiang and Li 2005).

Because the circulation anomalies over central Asia and the simultaneous arrival of tropical ISOs at the NISM are favorable conditions for the occurrence of extreme phases over the NISM, both the timing of the initiation of the two systems and their phase relationship seem to be critical for the occurrence of extreme phases. When the two systems are not adequately

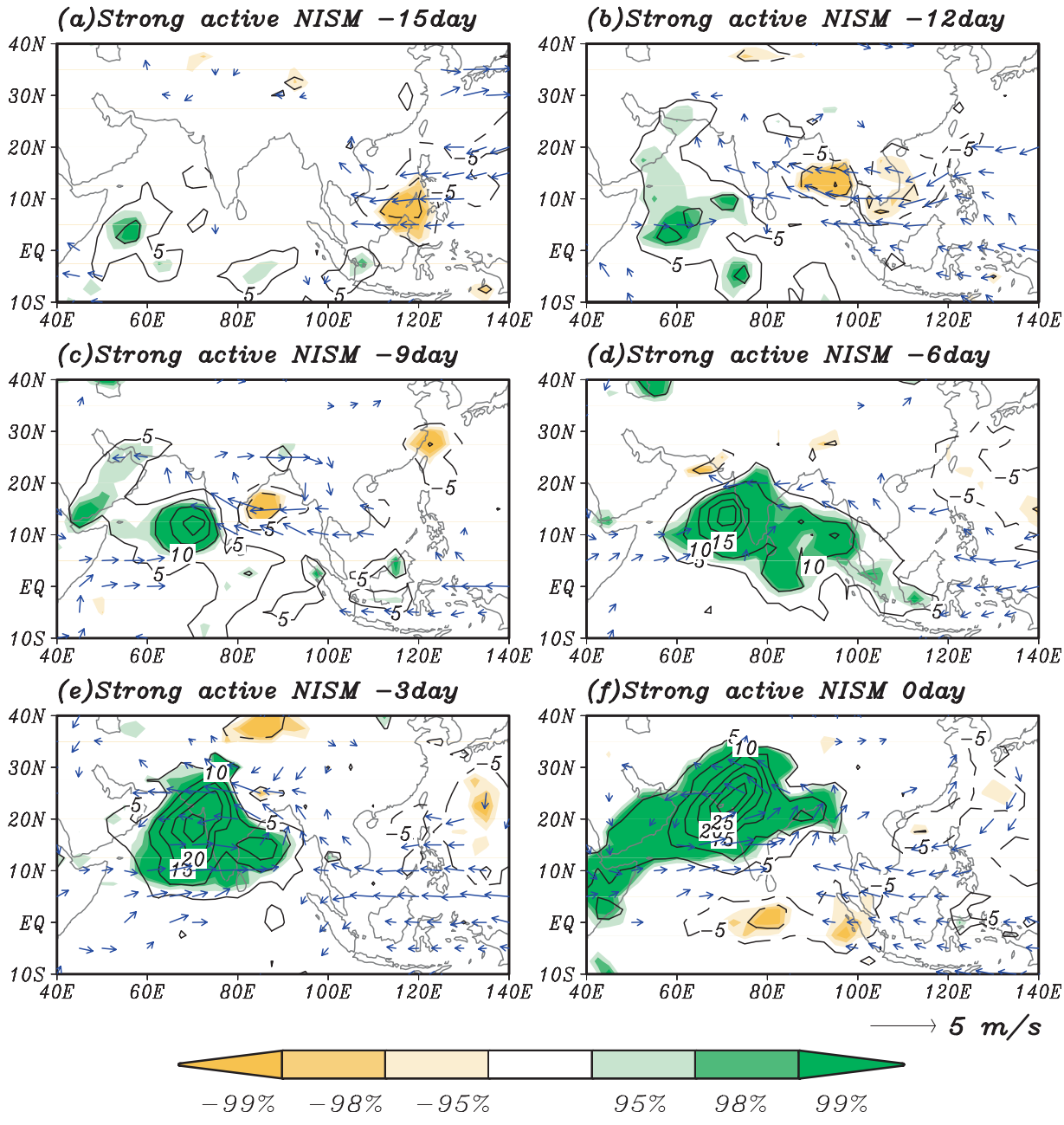

FIG. 8. As in Fig. 4, but for the 50 NISM strong (but not extremely) active phases.

collaborated, the effects from the tropics and the midlatitude do not influence the NISM in chorus, and, therefore, the convective intensity of NISM has less of a chance of reaching the extreme stage. The strong phases of the NISM, which are defined by an NISM OLR that is larger than 1.0 but less than 1.7 standard deviation, may tend to occur when the phases of the two systems are mismatched and, if so, may need to be compared with extreme phases. Such a comparison will shed light on the importance of the timing of leading systems on the occurrence of the extreme phases of the NISM.

The evolution and structure of 50 strong, active NISMs is detailed in the composite figures of OLR and 200-hPa circulation anomalies from day −15 to day 0. Apparent in Figs. 8 and 9 is that the tropical ISOs and midlatitude wave train preceding strong active phases are much less significant and of a shorter duration than those preceding extreme phases, possibly because of the diversification of the leading flows prior to the strong

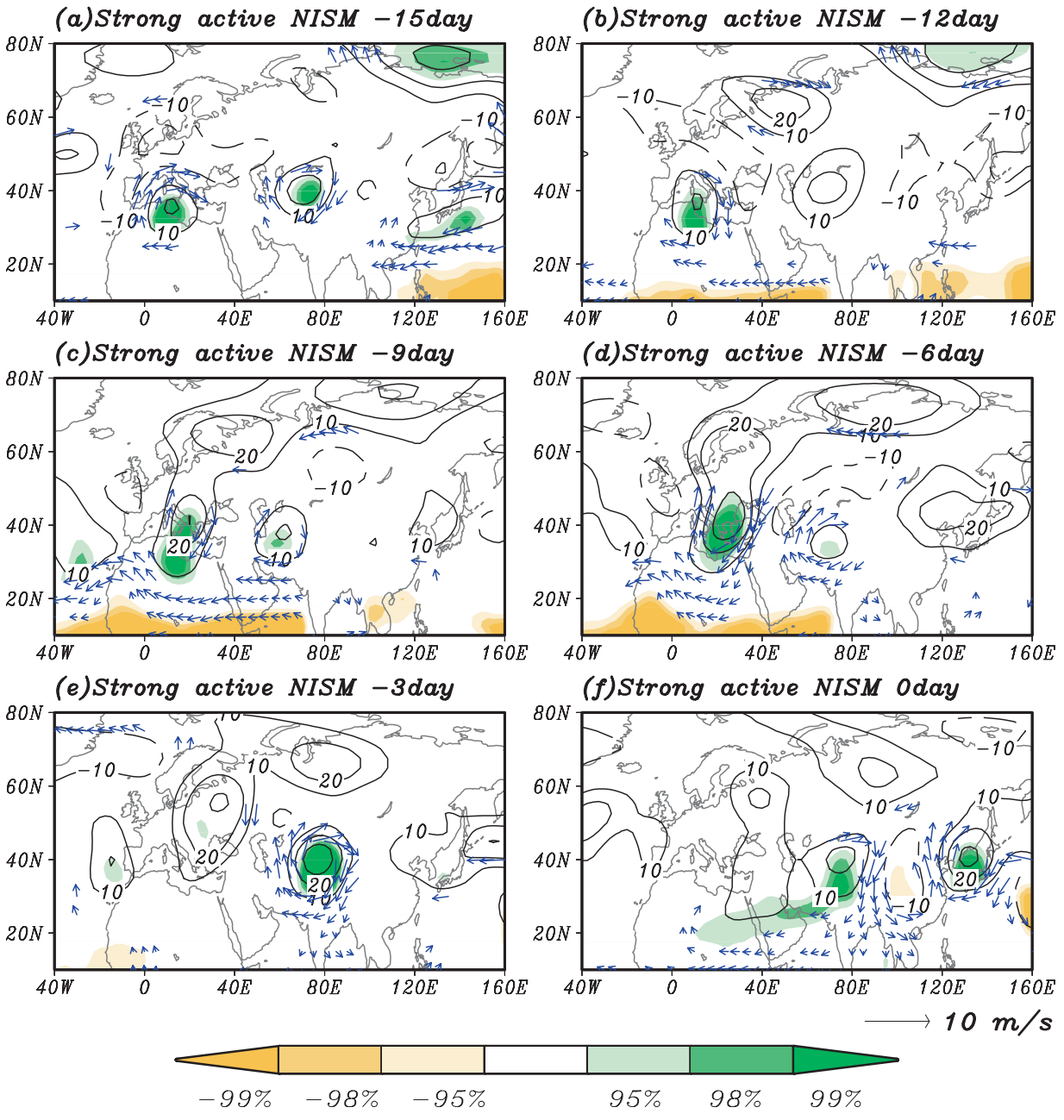

FIG. 9. As in Fig. 5, but for the 50 NISM strong (but not extremely) active phases.

active NISM. This difference is particularly apparent for the extratropical circulation. The smaller magnitude and extent of an anomalous high over central Asia may be associated with the disappearance of the Rossby wave train migrating from northwestern Europe to central Asia. The antecedent tropical convective band is confined over the Indian Ocean and is less extensive than its counterpart for the extremely active phase, while its origin can be traced back to the eastern EIO at day −15.

The evolution of OLR and extratropical circulation for 57 strong break NISM events is now considered (Figs. 10 and 11). The propagation of the wave train from the west Siberian plain to central Asia is observed in day −6 (Fig. 11). The OLR over the NISM region appears to develop locally from day −6 to day 0 without significant intrusion of the tropical 30–60-day ISOs (Fig. 10). The only significant leading feature in OLR is 10–20-day ISOs propagating westward from the Bay of Bengal to India from day −6 to day −3. Without the

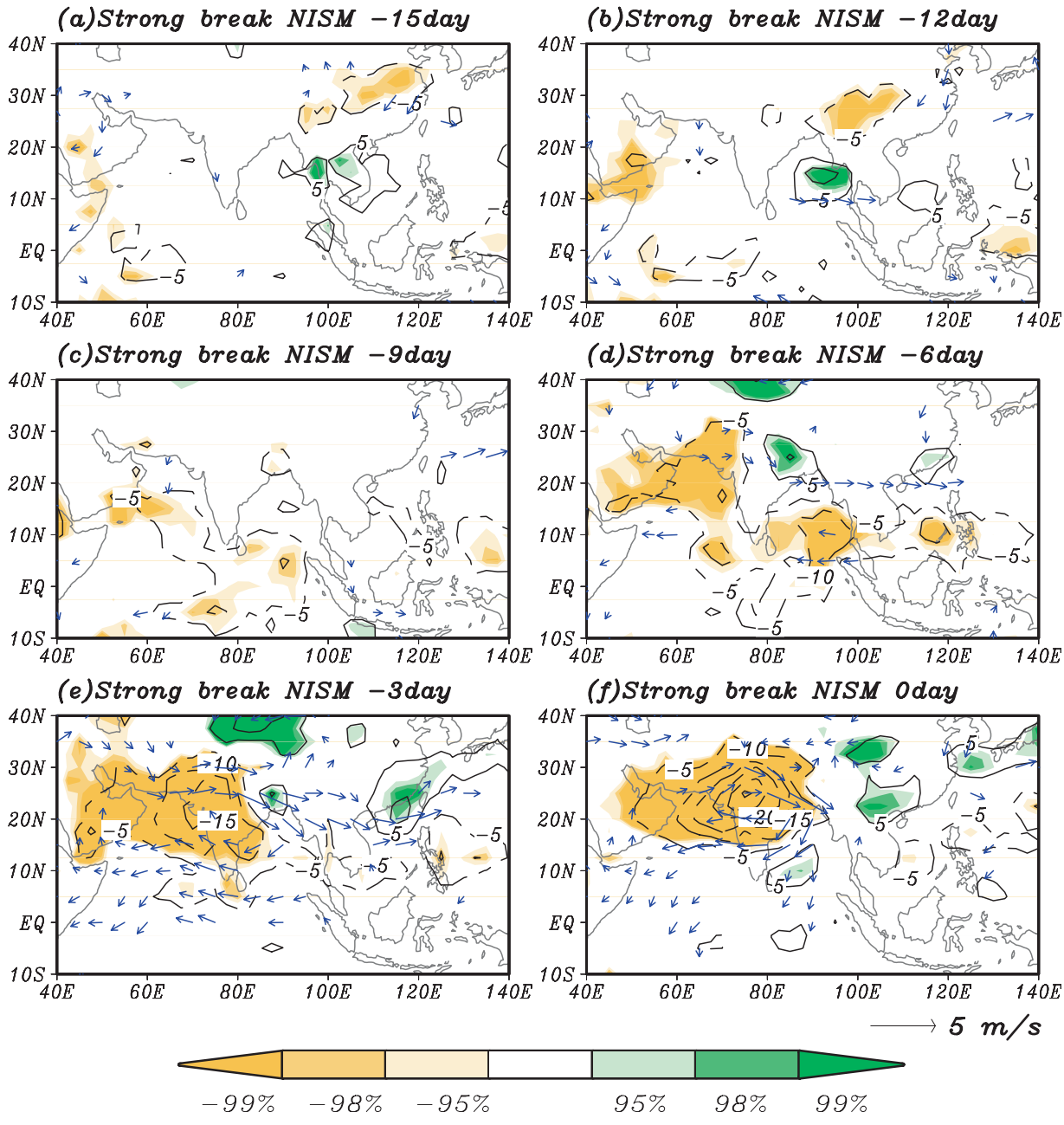

FIG. 10. As in Fig. 4, but for the 57 NISM strong (but not extremely) break phases.

joining of 30–60-day ISOs, the strong anomalous low over central Asia with a comparable magnitude to its counterpart for extreme break phases seems inadequate to induce the extremely dry phase over the NISM.

The appropriate timing of tropical ISOs and the midlatitude wave train provides a time window favorable for the occurrence of an extreme phase. In the absence of this matched timing, neither the tropical ISO nor the circulation anomaly over central Asia alone is sufficient to support unstable growth of convection to an extreme stage.

5. Feasibility of forecasting the extreme phases

Because of the serious outcomes of these extreme phases, it is of great practical and theoretical interest to explore the feasibility of forecasting an extreme phase. Based on the composite map of extreme phases (Figs. 4–7),

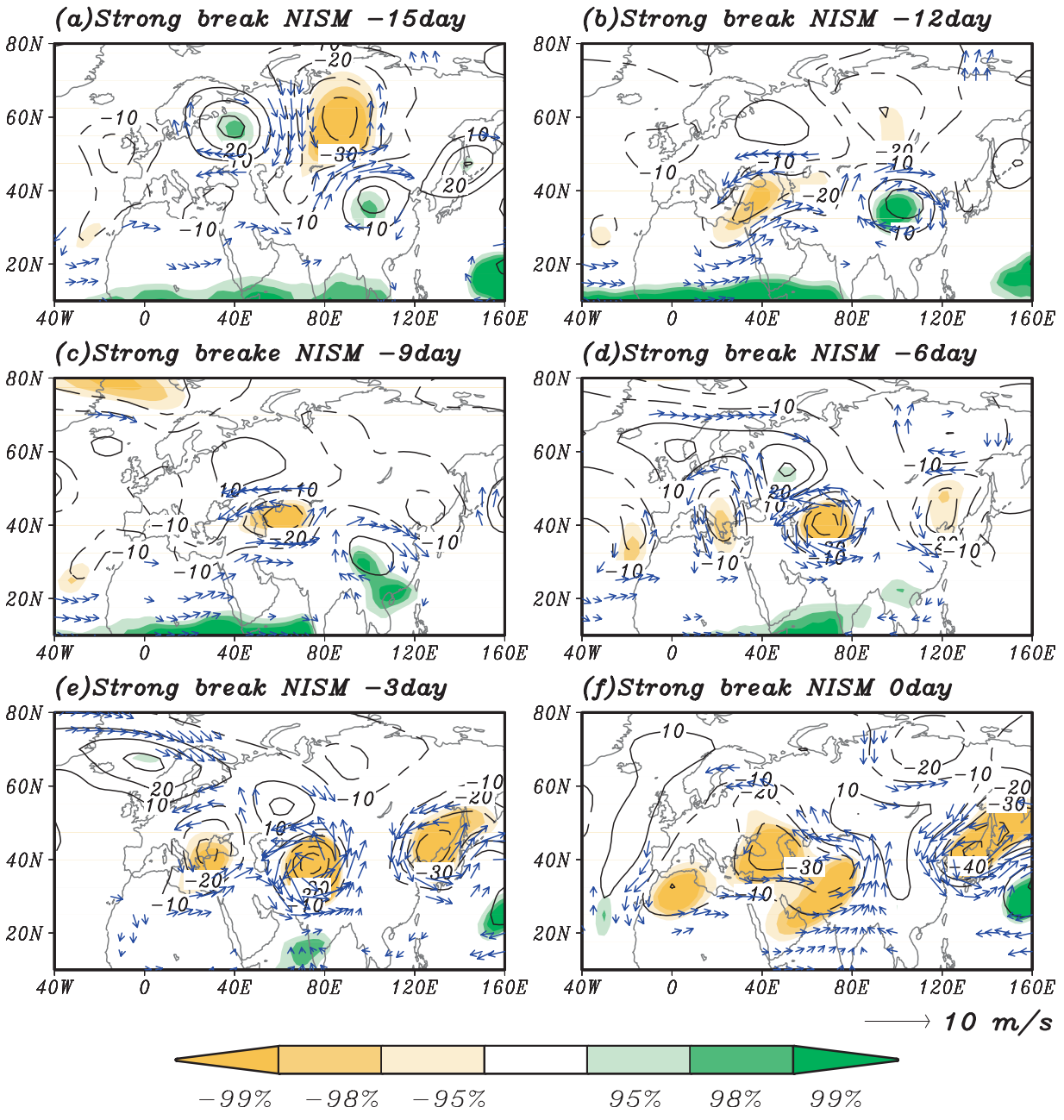

FIG. 11. As in Fig. 5, but for the 57 NISM strong (but not extremely) break phases.

two precursors are selected to forecast the convective activity over the NISM. One is the OLR predictor averaged within the domain (5°–15°N, 60°–95°E), which can capture the large-scale tropical ISO activity originating from the EIO. The other is the area-averaged 200-hPa geopotential height (GH) predictor over central Asia (32.5°–42.5°N, 65°–85°E), which describes the effect of the extratropics on the NISM. Both predictors are normalized by their corresponding standard deviation. A joint predictor is constructed by averaging the two nondimensional predictors to measure the combined effect of the tropics and extratropics on the NISM.

Figure 12 shows the lead–lag correlation between each predictor and the NISM OLR with a lag of up to 15 days. With the OLR predictor alone, the correlation with the NISM reaches a maximum (0.48) when it leads the NISM OLR by 4–6 days. The GH predictor yields a maximum correlation of 0.5 when it leads the NISM OLR by 3–4 days. The combined predictor shows a

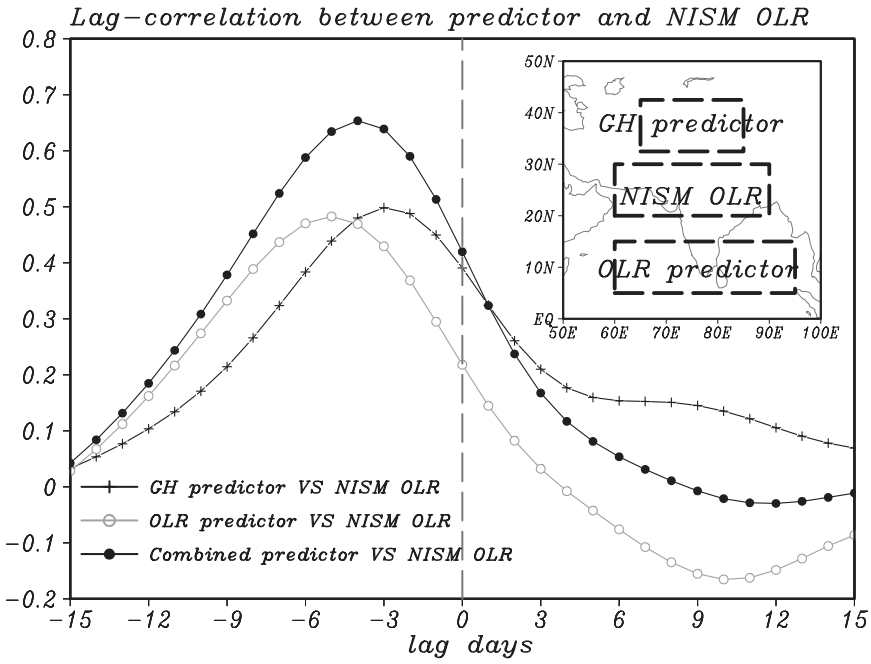

FIG. 12. Lead–lag correlation coefficients between three predictors (GH predictor, OLR predictor, and the combined GH–OLR predictor) and the predictand, namely, the NISM OLR index. The negative lag days show that the predictor leads the predictand. The sign of OLR anomalies is reversed. The domains of GH and OLR predictors are shown in the embedded map.

greater correlation (0.65) at a lead time of about 4–5 days, suggesting a strong capability of the combined predictor to forecast convection variability in the NISM region. Therefore, the two somewhat independent and complementary predictors combine together, resulting in a predictor that shows superior ability than either of them alone and accounts for almost 40% of the variability of the NISM OLR. This combined predictor also maintains a good balance between a large correlation skill (0.65) and acceptable prediction lead time (4–5 days).

It is possible to maximize the correlation between the predictors and predictand, but at the expense of shortening of the forecast lead time. The multiregression with the OLR and GH predictors was tested, and it was found that the simple average of two predictors with equal weighting has the best performance, suggesting that the tropics and extratropics have comparable influence on the ISOs in the NISM.

For 35 extremely active and 28 extreme break phases selected in this study, the corresponding GH and OLR predictors have the absolute mean value of 0.9 at 4–5 days lead time, and almost 45% of these extreme phases have at least one predictor exceeding 1.0.

The combined predictor can explain 40% of the predictand variance at a lead time of 4–5 days. Thus, it is expected that 40% of the extreme phases can be predicted by this combined predictor. We thus propose a simple prediction scenario for forecasting the extreme NISM phase about 4–5 days in advance. The date on which one anticipates occurrence of the peak day of an extreme phase over the NISM is the day on which the combined predictor is greater than 1.0. From 1979 to 2006, there are a total of 53 (hits + false alarms) occasions that satisfy this scenario. Within 10 days after the forecast date, 22 of them developed into an extremely active phase (the hit rate is about 63%). Eleven of the 53 occasions grew to a strong active phase but did not reach the extreme phases. On average, 42% of the events captured by this prediction scenario successfully developed to the extremely active phase. Note that our forecast day is the first day on which the combined predictor exceeds 1.0, not the day on which the combined predictor reaches its maximum, and therefore the forecast lead time for the peak day of an extreme phase extends 6–7 days, which is longer than the 4–5-day lead time between the combined predictor and predictand revealed in lead–lag correlation analysis (Fig. 12). The average duration of the extreme phases is about 4–5 days. Generally, an extreme phase starts 2 days earlier than the occurrence of peak day. Thus, our prediction scenario can predict, 4–5 days in advance, the beginning

TABLE 1. Performance of simple prediction scenario for the NISM's extremely active phase with choice of different threshold values (1.0–1.7). An NISM extremely active phase occurring within 10 days after the date of forecast is considered a successful forecast (hit). Extreme phase that is not forecast by this scenario is considered a miss. Extreme phase that is forecast to occur, but does not occur is considered as false alarm. Hit rate is defined as the ratio of hits to sum of hits and misses. False alarm ratio is the ratio of false alarms to sum of hits and false alarms. Threat score is defined as the ratio of hits to sum of hits, misses, and false alarms. The hit rates, false alarm ratio, threat score, and averaged predictive lead time provided by the scenario are important criteria that show the forecast capability of the scenario.

Threshold	Hit	Miss	False alarm	Hit rate	False alarm ratio	Threat score	Predictive lead time
1.0	22	13	31	63%	58%	33%	6–7 days
1.1	15	20	20	43%	57%	27%	6–7 days
1.2	13	22	14	37%	52%	27%	5–6 days
1.3	12	23	13	34%	52%	25%	5–6 days
1.4	9	26	10	26%	53%	20%	5–6 days
1.5	9	26	4	26%	30%	23%	5–6 days
1.6	8	27	2	23%	20%	22%	5–6 days
1.7	6	29	1	17%	14%	17%	5–6 days

TABLE 2. Same as in Table 1, but for the NISM extreme break phases.

Threshold	Hit	Miss	False alarm	Hit rate	False alarm ratio	Threat score	Predictive lead time
−1.0	21	8	34	72%	62%	33%	6–7 days
−1.1	16	13	20	55%	56%	33%	6–7 days
−1.2	15	14	16	52%	52%	33%	5–6 days
−1.3	8	21	11	28%	58%	20%	5–6 days
−1.4	6	23	8	21%	57%	16%	5–6 days
−1.5	6	23	5	21%	45%	18%	5–6 days
−1.6	7	22	2	24%	22%	23%	5–6 days
−1.7	5	24	1	17%	17%	17%	5–6 days

of an extreme phase. For extreme break phases, this scenario showed a similar skill.

Sensitivity tests were carried out to examine how the forecast capability of the scenario varies with the choice of the threshold value (Tables 1 and 2). When we chose a threshold value of 1.3, 25 events were hindcast (hits + false alarms), and 12 (hits) out of 25 events developed into an extremely active phase (Table 1). When this value was increased to 1.7, only seven (hits + false alarms) events satisfied the scenario, and six (hits) of them were extremely active phases. The scenario with a larger threshold value has a lower false alarm ratio, but at the expense of an increased missing rate and decreasing threat score. An event forecast by a scenario with a moderate threshold value (1.0–1.2) has a 40% probability of developing into an extreme phase, and the corresponding hit rate and threat score are high.

On average, only 1.25 extremely active phases and one extreme break phase occur during each summer season (which spans 122 days), and the duration of an extreme phase in each summer can last for about 5 days. Thus, the probability of an occurrence of such an extreme event period is rather small, less than 4%. Given this rather small probability of occurrence, our prediction scenario is skillful for forecasting the extreme phase.

The data used to test this simple hindcast has been processed by three filters. Note that removal of the climatological seasonal cycle can be performed in a real-time forecast, assuming that the seasonal cycle is ''invariant.'' The 5-day running mean filter may be replaced by a spatial filter to remove high-frequency variability to some extent. Only the interannual variability is difficult to remove. Given that the interannual variance of the ISM is much less than its intraseasonal counterpart (Krishnamurthy and Shukla 2000), this prediction scenario can be used for a real-time forecast without excluding the interannual variability.

6. Summary and discussion

a. Summary

This study reveals tropical and extratropical precursors associated with the extreme active and break phases of the northern ISM (NISM; 20°–30°N, 60°–90°E). The OLR and 200-hPa geopotential height are used to measure the tropical convection activity and midlatitude circulation anomalies, respectively. The extreme phases were defined using area-mean OLR index exceeding 1.7 standard deviation.

Our composite analysis indicates that two prominent atmospheric processes lead the extreme phases over the northern ISM. One is the development of the upper-tropospheric anomalous circulation over central Asia to the north of the NISM. This extratropical precursor appears to be induced by a large-scale Rossby wave train emanating from the northwestern Europe to central Asia via the western Siberia plain. The other process is the collective influence of a northward propagation of the 30–60-day ISO from the equatorial Indian Ocean and a westward propagation of the 10–20-day disturbance from the South China Sea. The tropical and extratropical processes can individually induce relatively strong convection anomalies over the NISM. However, when the central Asian anomalous high (low) coincides with the arrival of the enhanced (suppressed) convection of the tropical ISOs, the collaboration of the tropical ISO and midlatitude wave train creates a favorable condition for the occurrence of the NISM

extremely active (break) phases, possibly resulting in severe flooding (drought) events. The appropriate timing of the two precursory systems is essential for the occurrence of the extreme phases. If the two leading systems are mismatched, the convective phase over the NISM barely develops to an extreme stage. Most of the NISM active and break phases with relatively strong, but not extreme, intensity are related to this inappropriate timing of tropical–extratropical interaction.

For the extreme phases over the southern ISM (SISM), the 30–60-day tropical ISOs initiated from the eastern EIO play a dominant role in controlling the convective condition over the SISM. The influence of the extratropical circulation is hard to extend south of 20°N to affect the extreme phases in the SISM.

Because of the severe outcomes of the extreme phases, the prediction of the extreme phases has the greatest economic benefit. In the light of the above findings, we have attempted to determine the potential of forecasting the extreme phases of the NISM. The area-averaged 200-hPa geopotential height anomalies over central Asia (32.5°–42.5°N, 65°–85°E) and the OLR anomalies over the Indian Ocean (5°–15°N, 60°–95°E) are selected to be the two predictors to represent the effects from the tropics and extratropics, respectively. The averaged value of the two predictors (normalized by their corresponding standard deviations) shows a skill that is higher than each individual predictor. Almost 40% of the intraseasonal variance of the NISM OLR is explained by this simple combined predictor at 4–5-days lead time.

A simple prediction scenario is designed to forecast the peak day of the NISM extreme phase 6–7 days in advance. Once this combined predictor increases monotonically up to 1.0, it is time to forecast an occurrence of the peak day of the NISM extreme phase after 6–7 days. Measures of prediction skill indicate that the best hit rate and threat score are obtained when the threshold value ranging from 1.0 to 1.2 is used. Generally, an event forecasted by this simple scenario has a probability of 40% to develop to an extreme phase. This significant statistical forecast may allow farming and hydrological communities to benefit from the predictive lead times involved.

b. Discussion

The correlation coefficient between the OLR predictor and geopotential height predictor is negligibly small, suggesting that the tropical ISOs vary independently from the circulation anomalies over central Asia. Thus, the extreme phases over the NISM often occur by chance. Extreme phases occur only about 2.25 times (1.25 extremely active and 1 extremely break phases) in 1 yr on average, and their timing is random within the summer season. Depending on the phase relationship of tropical–extratropical interaction, for some years there is an absence of the extreme phase, while in some years several extreme phases are seen. In this manner, interannual variations in the frequency of extreme phase are random and are therefore governed by stochastic statistics.

An application of our result concerns the predictability of intraseasonal variability of the ISM. Because the NISM is one such area that exhibits a strong coupling between the tropics and extratropics, the predictability of the ISO over the NISM is largely degraded under the influence from the extratropics. To better predict the ISO activity over the NISM, the extratropical effect must be taken into account in the empirical and dynamical prediction scheme. The performance of a dynamical model in capturing the observed tropical–extratropical interaction is an important criterion to test whether a dynamical model can be used to predict the NISM extreme phases.

The ISM rainfall shows significant temporal variations extending from synoptic to intraseasonal, interannual, decadal, and longer time scales. Because multiple time scales are involved in affecting the occurrence of the extreme phases, the interaction between different time scales adds complexity to the attribution. The relationship between the interannual variation in the frequency and intensity of extreme phases and interannual variability of the ISM rainfall is one interesting issue to explore in the future. The interaction between extreme active and break phases of the ISM and the occurrence of the extreme precipitation events are rarely documented, and thus this is another interesting topic for the future study.

Our prediction scenario shows promising skill in predicting the extreme phases, but it is also noted that a large number of false alarm events are associated with moderate thresholds and many miss events are generated by using higher thresholds (Tables 1 and 2). This is a severe limitation on the usefulness of our method. Further study could be necessary to examine these cases to see whether new predictor can be revealed. An additional problem remains that our prediction scenario is designed based on the large-scale feature of the preceding systems of the extreme phase. Some synoptic- and subsynoptic-scale systems and their interaction with large-scale circulation may be responsible for the development of the extreme phases. A large portion of miss and false alarm events in our hindcast experiment may be related to these unidentified processes.

This work is the first study to emphasize the importance of exploring the predictability of the ISM's

extreme active and extreme break phases. Although the prediction scenario we propose has not been tested for operational applications, it encourages further investigation into better forecast schemes to predict extreme monsoon ISO events.

Acknowledgments. This study has been supported by the National Science Foundation/Climate Dynamics Program Award ATM-0647995. The authors appreciate the anonymous reviewers' comments on an early version of the manuscript, which lead to significant improvement.

REFERENCES

Annamalai, H., and J. M. Slingo, 2001: Active/break cycles: Diagnosis of the intraseasonal variability of the Asian summer monsoon. *Climate Dyn.,* **18,** 85–102.

Bell, M., A. Giannini, E. Grover-Kopec, B. Lyon, and C. Ropelewski, Eds., 2006: Climate impacts—August. *IRI Climate Digest,* September 2006, Columbia University. [Available online at http://iri.columbia.edu/climate/cid/Sep2006/impacts.html#SAsia.]

De, U. S., R. K. Dube, and G. S. P. Rao, 2005: Extreme weather events over India in the last 100 years. *J. Indian Geophys. Union,* **9,** 173–187.

Ding, Q. H., and B. Wang, 2007: Intraseasonal teleconnection between the summer Eurasian wave train and the Indian monsoon. *J. Climate,* **20,** 3751–3767.

Gadgil, S., 1995: Climate change and agriculture: An Indian perspective. *Curr. Sci.,* **69,** 649–659.

——, and P. R. S. Rao, 2000: Famine strategies for a variable climate—A challenge. *Curr. Sci.,* **78,** 1203–1215.

——, and P. V. Joseph, 2003: On breaks of the Indian monsoon. *Proc. Indian Acad. Sci. Earth Planet. Sci.,* **112,** 529–558.

——, P. R. S. Rao, and K. N. Rao, 2002: Use of climate information for farm level decision making: Rainfed groundnut in southern India. *Agric. Syst.,* **74,** 431–457.

Gill, A. E., 1980: Some simple solutions for heat induced tropical circulation. *Quart. J. Roy. Meteor. Soc.,* **106,** 447–462.

Goswami, B. N., 2005: South Asian monsoon, *Intraseasonal Variability of the Atmosphere-Ocean Climate System,* K. M. Lau and D. E. Waliser, Eds., Springer Praxis, 19–61.

——, and R. S. A. Mohan, 2001: Intra-seasonal oscillations and predictability of the Indian summer monsoon. *Proc. Indian Natl. Sci. Acad.,* **67A,** 369–383.

Hartmann, D. L., and M. L. Michelson, 1989: Intraseasonal periodicities in Indian rainfall. *J. Atmos. Sci.,* **46,** 2838–2862.

Huffman, G. J., R. F. Adler, M. M. Morrissey, S. Curtis, R. Joyce, B. McGavock, and J. Susskind, 2001: Global precipitation at one-degree daily resolution from multi-satellite observations. *J. Hydrometeor.,* **2,** 36–50.

Jiang, X., and T. Li, 2005: Re-initiation of the boreal summer intraseasonal oscillation in the tropical Indian Ocean. *J. Climate,* **18,** 3777–3795.

Joseph, S., A. K. Sahai, and B. N. Goswami, 2008: Eastward propagating MJO during boreal summer and Indian monsoon droughts. *Climate Dyn.,* doi:10.1007/s00382-008-0412-8.

Kanamitsu, M., W. Ebisuzaki, J. Woollen, S.-K. Yang, J. J. Sling, M. Fiorino, and G. L. Potter, 2002: NCEP–DOE AMIP-II Reanalysis (R-2). *Bull. Amer. Meteor. Soc.,* **83,** 1631–1643.

Kemball-Cook, S., and B. Wang, 2001: Equatorial waves and air–sea interaction in the boreal summer intraseasonal oscillation. *J. Climate,* **14,** 2923–2942.

Kripalani, R. H., A. Kulkarni, and S. V. Singh, 1997: Association of the Indian summer monsoon with the Northern Hemisphere mid-latitude circulation. *Int. J. Climatol.,* **17,** 1055–1067.

Krishnamurthy, V., and J. Shukla, 2000: Intraseasonal and interannual variability of rainfall over India. *J. Climate,* **13,** 4366–4377.

——, and ——, 2007: Intraseasonal and seasonally persisting patterns of Indian monsoon rainfall. *J. Climate,* **20,** 3–20.

——, and ——, 2008: Seasonal persistence and propagation of intraseasonal patterns over the Indian monsoon region. *Climate Dyn.,* **30,** 353–369.

Krishnamurti, T. N., and H. N. Bhalme, 1976: Oscillations of a monsoon system. Part I: Observational aspects. *J. Atmos. Sci.,* **33,** 1937–1954.

——, and D. Subrahmanyam, 1982: The 30-50 day mode at 850 mb during MONEX. *J. Atmos. Sci.,* **39,** 2088–2095.

Krishnan, R., C. Zhang, and M. Sugi, 2000: Dynamics of breaks in the Indian summer monsoon. *J. Atmos. Sci.,* **57,** 1354–1372.

Murakami, T., T. Nakazawa, and J. He, 1984: On the 40–50 day oscillation during 1979 Northern Hemisphere summer. Part 1: Phase propagation. *J. Meteor. Soc. Japan,* **62,** 440–468.

Raghavan, K., 1973: Break-monsoon over India. *Mon. Wea. Rev.,* **101,** 33–43.

Rajeevan, M., J. Bhate, J. D. Kale, and B. Lal, 2006: High resolution daily gridded rainfall data for the Indian region: Analysis of break and active monsoon spells. *Curr. Sci.,* **91,** 296–306.

——, S. Gadgil, and J. Bhate, 2008: Active and break spells of the Indian summer monsoon. National Climate Centre Research Rep. 6, Indian Meteorological Department, Pune, 46 pp. [Available online at www.imdpune.gov.in.]

Ramamurthy, K., 1969: Monsoon of India: Some aspects of "break" in the Indian South west monsoon during July and August. Forecasting Manual, Part IV.18.3, Indian Meteorological Department, New Delhi, 29 pp.

Raman, C. R. V., and Y. P. Rao, 1981: Blocking highs over Asia and monsoon droughts over India. *Nature,* **289,** 271–273.

Ramaswamy, C., 1962: Breaks in the Indian summer monsoon as a phenomenon of interaction between the easterly and the subtropical westerly jet streams. *Tellus,* **14A,** 337–349.

Rao, Y. P., 1976: *Southwest Monsoon. Meteor. Monogr.,* No. 1, Indian Meteorological Department, 366 pp.

Rodwell, M. J., and B. J. Hoskins, 1996: Monsoons and the dynamics of deserts. *Quart. J. Roy. Meteor. Soc.,* **122,** 1385–1404.

Sikka, D. R., 1999: Monsoon drought in India. Center for Ocean–Land–Atmosphere Studies, Joint COLA/CARE Tech. Rep. 2, 270 pp.

——, and S. Gadgil, 1980: On the maximum cloud zone and the ITCZ over Indian longitudes during the southwest monsoon. *Mon. Wea. Rev.,* **108,** 1840–1853.

Unninayar, M. S., and T. Murakami, 1978: Temporal variations in the northern hemispheric summer circulations. *Indian J. Meteor. Hydrol. Geophys.,* **29,** 170–186.

Wang, B., and H. L. Rui, 1990: Synoptic climatology of transient tropical intraseasonal convection anomalies: 1975–1985. *Meteor. Atmos. Phys.,* **44,** 43–61.

——, and X.-S. Xie, 1996: Low-frequency equatorial waves in vertically sheared zonal flow. Part I: Stable waves. *J. Atmos. Sci.,* **53,** 449–467.

——, P. J. Webster, and H. Teng, 2005: Antecedents and self-induction of the active-break south Asian monsoon unraveled

by satellites. *Geophys. Res. Lett.,* **32,** L04704, doi:10.1029/2004GL020996.

Webster, P. J., and C. Hoyos, 2004: Prediction of monsoon rainfall and river discharge variability on 15–30-day time scales. *Bull. Amer. Meteor. Soc.,* **85,** 1745–1765.

——, V. O. Magana, T. N. Palmer, J. Shukla, R. T. Tomas, M. Yanai, and T. Yasunari, 1998: Monsoons: Processes, predictability and the prospects of prediction. *J. Geophys. Res.,* **103,** 14 451–14 510.

Wilks, D. S., 1995: *Statistical Methods in the Atmospheric Sciences: An Introduction*. Academic Press, 467 pp.

Xie, P., and P. A. Arkin, 1997: Global precipitation: A 17-year monthly analysis based on gauge observations, satellite estimates, and numerical model outputs. *Bull. Amer. Meteor. Soc.,* **78,** 2539–2558.

Xie, X.-S., and B. Wang, 1996: Low-frequency equatorial waves in vertically sheared zonal flow. Part II: Unstable waves. *J. Atmos. Sci.,* **53,** 3589–3605.

Yasunari, T., 1979: Cloudiness fluctuation associated with the Northern Hemisphere summer monsoon. *J. Meteor. Soc. Japan,* **57,** 227–242.

——, 1980: A quasi-stationary appearance of 30–40 day period in the cloudiness fluctuation during summer monsoon over India. *J. Meteor. Soc. Japan,* **58,** 225–229.

——, 1981: Structure of an Indian summer monsoon system with around 40-day period. *J. Meteor. Soc. Japan,* **59,** 336–354.